Article

Mapping the Dabus Wetlands, Ethiopia, Using Random Forest Classification of Landsat, PALSAR and Topographic Data

Pierre Dubeau [1],* [ID]**, Douglas J. King [1], Dikaso Gojamme Unbushe [2]** [ID] **and Lisa-Maria Rebelo [3]**

[1] Department of Geography and Environmental Studies, Carleton University, 1125 Colonel By Drive, Ottawa, ON K1S 5B6, Canada; doug.king@carleton.ca or DougJKing@cunet.carleton.ca
[2] Department of Biology, College of Natural Sciences, Arba Minch University, Arba Minch, Ethiopia; unbusheg@gmail.com
[3] International Water Management Institute, IWMI-Southeast Asia, P.O. Box 4199, Vientiane 1009, Laos; l.rebelo@cgiar.org
* Correspondence: pierdubo@gmail.com; Tel.: +1-778-971-6363

Abstract: The Dabus Wetland complex in the highlands of Ethiopia is within the headwaters of the Nile Basin and is home to significant ecological communities and rare or endangered species. Its many interrelated wetland types undergo seasonal and longer-term changes due to weather and climate variations as well as anthropogenic land use such as grazing and burning. Mapping and monitoring of these wetlands has not been previously undertaken due primarily to their relative isolation and lack of resources. This study investigated the potential of remote sensing based classification for mapping the primary vegetation groups in the Dabus Wetlands using a combination of dry and wet season data, including optical (Landsat spectral bands and derived vegetation and wetness indices), radar (ALOS PALSAR L-band backscatter), and elevation (SRTM derived DEM and other terrain metrics) as inputs to the non-parametric Random Forest (RF) classifier. Eight wetland types and three terrestrial/upland classes were mapped using field samples of observed plant community composition and structure groupings as reference information. Various tests to compare results using different RF input parameters and data types were conducted. A combination of multispectral optical, radar and topographic variables provided the best overall classification accuracy, 94.4% and 92.9% for the dry and wet season, respectively. Spectral and topographic data (radar data excluded) performed nearly as well, while accuracies using only radar and topographic data were 82–89%. Relatively homogeneous classes such as Papyrus Swamps, Forested Wetland, and Wet Meadow yielded the highest accuracies while spatially complex classes such as Emergent Marsh were more difficult to accurately classify. The methods and results presented in this paper can serve as a basis for development of long-term mapping and monitoring of these and other non-forested wetlands in Ethiopia and other similar environmental settings.

Keywords: wetlands; Random Forest; classification; Landsat; PALSAR; L-band; DEM; Ethiopia

1. Introduction

Wetlands are among the most biologically productive ecosystems in the world. Their rich biodiversity contributes to sustaining ecosystem functions and services [1] and in regulating and storing water. Tropical wetlands in Africa are often key to maintaining livelihoods [2], but threats to wetlands from anthropogenic pressures can be significant. Wetlands also contribute significantly to carbon sequestration as much of the permanently flooded swamps in tropical Africa are dominated by papyrus sedge (*Cyperus papyrus*) [3], which has productivity comparable to that of forest [4].

Global assessment of wetlands shows that their extent, composition, and condition are still poorly understood [1,5–7].

In the Ethiopian highlands where access to water is generally limited, particularly during the dry season, wetlands play a key role in regulating the hydrologic cycle and improving water availability and quality [8,9]. The establishment of a national inventory and information on the extent, distribution, and characteristics of wetland ecosystems is still in its infancy as there is a paucity of information about some of the country's key wetlands, including the Dabus wetlands, which are the focus of this study. Until recently, knowledge about the significance of the Dabus wetlands was lacking, despite the fact that they include large papyrus swamps supporting a rich biodiversity [10,11], while farmers and pastoralists benefit from their provision of water during the dry season.

Remote sensing technologies can provide up-to-date spatial and temporal information about wetlands [12], thereby contributing to sustainable wetland management [13]. Multispectral optical and synthetic aperture radar (SAR) data have been used extensively, either independently or in combination with topographic variables, to map and characterize wetland vegetation in many regions of the world for a variety of goals and applications [12,14–22]. Vegetation spectral reflectance in the visible, near-infrared (NIR) and mid- or short-wave infrared (SWIR) is a function of chlorophyll absorption for photosynthesis, structure, biomass and moisture [23,24], while SAR backscatter is dependent on surface roughness and moisture. SAR can detect smooth open water surfaces and discriminate different wetland plant and canopy structures [25,26]. The ability of radar to penetrate clouds, and to some extent, rain, as well as day and night operability are some of the key features that provide a distinct advantage over optical sensors, especially in tropical environments where frequent cloud cover prevails, especially during the rainy season [23,27]. Wetland plant community distributions are also generally dependent on hydrologic characteristics, which in turn depend to a large degree on topography. Local terrain attributes (e.g., slope and topographic wetness indices) [28,29] can be readily extracted from existing DEMs and combined with remote sensing data in wetland mapping and analysis.

The overall goal of this study was to demonstrate how the Dabus Wetlands, which are important ecosystems that are very challenging to access, can be effectively characterized and mapped using remote sensing and topographic data from multiple sources. This study builds on remote sensing wetland research examples drawn from tropical regions in the Congo Basin [30], South Africa [31,32], and the Amazon basin [33,34]. Emphasis was placed on a need to have free or relatively easy access to data and processing software. The specific research objectives were: (1) determine the relative importance of Landsat, PALSAR and topographic variables in thematic mapping of Dabus wetland classes; and (2) given marked differences between the dry and wet seasons, determine if data from one or both seasons is best for such classification.

2. Materials and Methods

2.1. Study Area

This research focuses on the headwater wetland ecosystems associated with the Dabus River, a large tributary of the Abay-Blue Nile River. The Dabus wetland complex is located in the central western region of Ethiopia (centered on 34°55′0″E, 9°15′0″N) in the administrative zones of West Wellega (Figure 1), which is part of the Sudano-Guinea zone [35]. It covers an area of approximately 80,000 ha and lies at an altitude of about 1300 m above sea level. The regional landscape surrounding the Dabus River is comprised of green vegetated hills dominated by cultivated fields. A protracted rainy season starts in March or April and can last to October, while peak rainfalls generally occur from June to September [36]. The mean annual rainfall reported for the study region is approximately 1414 mm; mean annual, minimum and maximum temperatures are 19.8 °C, 11.8 °C and 30.9 °C, respectively [37]. The upstream areas are waterlogged for most of the year while downstream areas are seasonally inundated but remain dry during the dry season. These wetlands present a rich

biodiversity, particularly in the generally inaccessible upstream areas as they have been least impacted by anthropogenic pressures. These upstream areas represent relatively pristine habitat that includes large perennially saturated papyrus swamps forming dense (3 to 5 m tall) canopies [38]. They also harbor a large population of common hippopotamus (*Hippopotamus amphibius*) estimated at several hundred individuals, as well as several rare bird species such as the Shoebill Stork (*Balaeniceps rex*) and the vulnerable Wattled Crane (*Bugeranus carunculatus* [39]) during the dry season field survey.
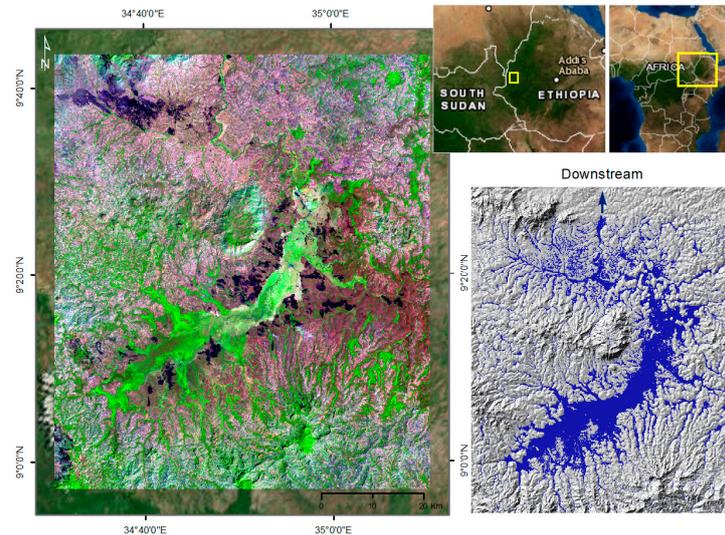

Figure 1. Geographic extent of the Dabus wetlands shown in a January 2010 Landsat-5 TM false color composite (RGB: bands 5, 4, and 3, respectively). The layout of the wetland is shown in blue overlaid on a shaded relief elevation model in the bottom right panel. Basemap image source: ESRI (Environmental Systems Research Institute) World Imagery.

The downstream areas are utilized by local farmers and pastoralists soon after the water recedes. As in other parts of Africa [40], areas of the Dabus wetlands are frequently burned followed by extensive grazing or seasonal agriculture. Expanses of tall emergent meadows covering the lower half of the Dabus wetlands are transformed into barren land by the end of the dry season (Figure 2c,d), but hydric soil conditions are nevertheless maintained as periods of inundation are sustained for several months each year. These areas present high abundance of annual C_4 grasses, which are adapted to fire and grazing [41], but floristic diversity is limited, especially where the most severe impacts have occurred.

2.2. Wetland Classes and Reference Data Collection

The wetland classes established for this study (Table 1) broadly follow the US wetland classification system [42]. Classes and descriptions were selected based on field observations at accessible locations and supplemented with visual interpretation of high resolution satellite imagery. Field surveys were carried out in July 2010 during the wet season and in March 2012 during the dry season (example photos in Figure 2) and included observation and analysis of hydro-geomorphology, ecology, plant community composition and structure, and land-use. Within each class, plant species composition, including abundance and dominance, was recorded, and plant functional types were identified. The general conditions of the Dabus wetlands did not change during the 19 months between the two surveys. No major disruption or large-scale conversion to commercial agricultural activities occurred. Land use practices that had the most impact on the wetlands included some incremental expansion of small-scale garden areas, which has been ongoing, while the burning of grasslands by local farmers and pastoralists was regarded as reoccurring events that can be difficult to predict and monitor. A burn class was included to account for such land use impacts.

A total of 255 ground reference locations were visited during the two field surveys. About 49% of the locations were visited twice to develop understanding of their wet-dry seasonal dynamics. There was a relatively balanced number of field locations across most classes, while the rarer or less accessible classes (i.e., Aquatic Bed and Shrub Marsh) could only be represented by a few locations. Shrub Marsh was present in less than 3% of the locations visited. Meadow Garden (MG) and Grass Marsh (GM) reference locations were interpreted from ESRI's world imagery and Google Earth in combination with an extensive collection of field photos (~2500 per trip). This approach was also used to augment the number of reference sample locations across all classes; the total number of reference locations from field visits and image interpretation was 1125 (Table 1). All reference sample locations were deemed to represent the given wetland class within a minimum area of about 3 × 3 Landsat pixels (90 m × 90 m). They were generally spatially well-distributed throughout the Dabus area and relatively balanced with respect to the land cover proportions observed across the main classes. The wetland classes averaged 80 reference locations per class, while the terrestrial classes averaged 140 locations. All reference pixel samples together represented about 1% of the study area, while their percent coverage for each main wetland class was: 14% (AB), 10% (WM), 5.4% (MG, ME, and GM), 11% (PS), 12.3% (SM), and 11.3% (FW). Burn patch reference locations (N = 49) were collected from the 12 January 2010 Landsat TM-5 image (see Section 2.3, Table 2). Table 1 provides generalized spectral information for each class, which was compiled as background information from analysis of the Landsat TM-5 and PALSAR L-band (HH/HV) pixels at each reference class location.
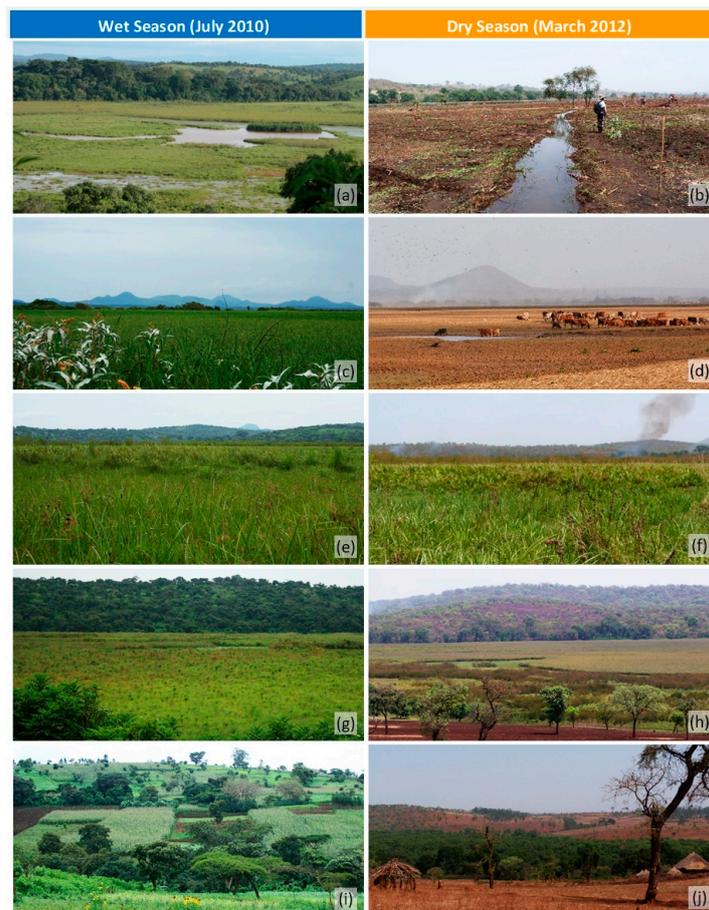

Figure 2. Example field photographs for: Aquatic Bed (**a**); Wet Meadow converted to cropland (**b**); Wet Meadow (**c**,**d**); Marsh Emergent (**e**,**f**); Papyrus Swamp (**g**); Papyrus Swamp and Shrub Marsh (**h**); Agriculture (maize) and Woodland (**i**); and forested area (centre) and fallow land (foreground) with houses/tukuls (**j**).

Table 1. Classes selected for thematic mapping and their general spectral characteristics. Total number of reference (Ref.) locations per class, and the percentage of the total that was surveyed in the field (%); 22% of reference locations were field surveyed.

Class Name	Class Code	Description	Optical/SAR (dB) Spectral Characteristics	Ref. N (%)
1. Aquatic Bed	AB	Vegetation growing on or below the surface, and areas of open water.	Lowest surface reflectance and backscatter intensity, across all classes.	78 (2.6%)
2. Wet Meadow	WM	Grass dominated but mixed with forbs and sedges; mostly found in low-lying areas; seasonally flooded (<3 months).	NDVI (0.4) with moderate-low variance; low backscatter intensity (−22).	90 (48%)
3. Meadow Garden	MG	Cultivated wetlands along narrow drainage channels formerly occupied by Wet Meadow, but also found in areas of drained/converted marshes.	Lowest NDVI (0.4) among wetlands, but very-high variance; 2nd highest backscatter intensity (−16) among wetland classes.	55 (15%)
4. Emergent Marsh	EM	Sedge dominated but mixed with grasses and forbs.	Moderate-high NDVI (0.5) and very-low backscatter (−23); low variance for both variables.	76 (24%)
5. Grass Marsh	GM	Mixed Grass/Sedge with forbs; seasonally flooded (<6 months).	Moderate NDVI (0.45) with very-low variance; lowest backscatter (−24) among herbaceous wetlands.	64 (67%)
6. Papyrus Swamp	PS	*Papyrus cyperus* dominated with ferns and other forbs.	Second highest NDVI (0.6) among wetlands with moderate variance (Q1–Q3: 0.52–0.63); high backscatter (−17).	99 (33%)
7. Shrub Marsh	SM	Fabaceae-shrub dominated marsh often associated with Papyrus Swamp.	High NDVI (0.55), backscatter moderate-high (−19) and shows clear separation with PS.	87 (8%)
8. Forested Wetland	FW	Woody forest seasonally inundated; dominated by *Syzygium guineense* with *Ficus sur* generally found along drainage channels.	Highest NDVI (0.65), also shared with Forest, and highest backscatter (−14) among all classes; very low variance.	98 (32%)
9. Woodland	WDL	Open/sparse canopy woody savannah-like vegetation with shrubs and scattered trees up to 10 m tall on grassy/herbaceous sub-layer	Moderate-low NDVI (0.45), markedly lower compared to Forested classes (FW and for); high backscatter (−16); low variance for both variables.	152 (17%)
10. Forest	FOR	Closed canopy broadleaf forest	Highest NDVI and backscatter (0.65 and −15, respectively), also shared with Forested Wetland; very low variance.	121 (12%)
11. Agriculture	AGR	Cropland, cultivated pasture, and homestead areas	Lowest NDVI (0.3) and backscatter (−19) among the terrestrial classes, excluding Burnt areas.	156 (19%)

2.3. Remotely Sensed Data Acquisition and Processing

As illustrated in the workflow diagram (Figure 3), the multi-source geospatial dataset assembled for this study included: Landsat 5 TM images; Advanced Land Observation Satellite (ALOS) Phase Array L-band Synthetic Aperture Radar (PALSAR) images (Table 2); vegetation and water indices derived from the Landsat data; and morphometric terrain parameters derived from a Shuttle Radar Topography Mission (SRTM) interferometric DEM (1 arc-second; nominal pixel size ~30 m at equator [43]).

Table 2. Landsat and PALSAR images used in wetland classification.

Year	Season	Landsat [1]	ALOS/PALSAR (Level 1.1/1.5)	ALOS/PALSAR 25-m Mosaic	Polarization
2011	Wet	14 October			
	Dry		10–27 January [2]		HH
2010	Wet	12 November	10–27 July [2]	10 October (East) and 27 July (West)	HH and HV
	Dry	12 January	7–24 January		HH
2009	Wet	9 November	7–24 July	7–24 July	HH and HV
	Dry				

[1] Landsat TM-5 Orbital Path (WRS): 171; Rows: 53 and 54; [2] PALSAR Process level 1.1.
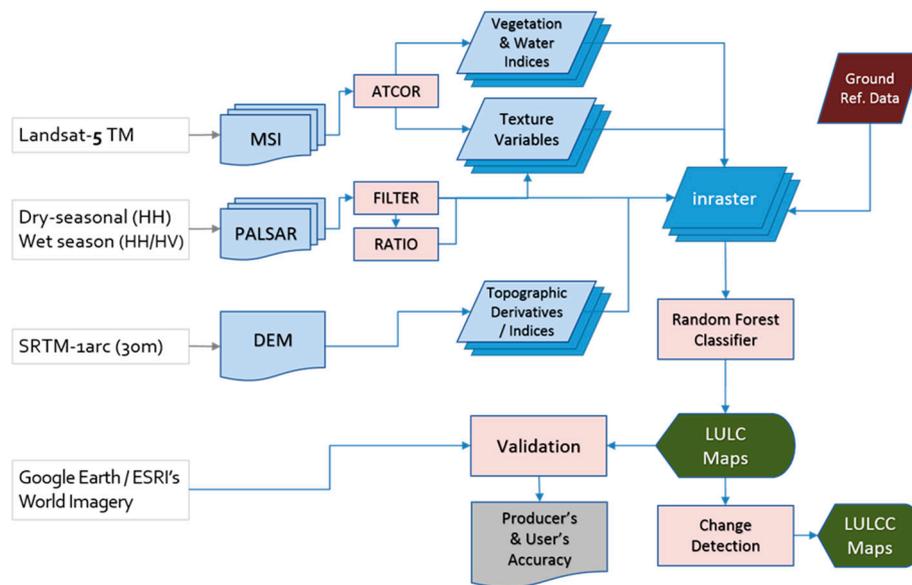
Figure 3. Summary of wetland classification workflow, from image pre-processing to final map product generation.

2.3.1. Landsat

Landsat imagery was acquired with Level 1T pre-processing [44] from NASA's Earth Observing System Data and Information System (EOSDIS) Worldview, Reverb ECHO, and the Earth Resources Observations and Science (EROS) archive Glovis Next (https://glovis.usgs.gov/). Dry season Landsat images were only available for 2010. Clouds and cloud shadows, as well as water were masked using the Fmask algorithm [45]. The ATCOR-2 algorithm was implemented [46] to correct for atmospheric and topographic effects, and to derive ground reflectance and surface temperature values from the multispectral and thermal bands, respectively, followed by production of mosaics of the image pairs using PCI Orthoengine.

2.3.2. PALSAR

PALSAR imagery was provided at no cost by the Japanese Exploration Agency JAXA, under the Wetland Theme of the ALOS Kyoto and Carbon Initiative (K & C) [47]. Two PALSAR scenes from consecutive orbital paths, 611 and 612, and row 170, were required for complete coverage of the Dabus wetlands, (Table 2). PALSAR images processed to Level 1.1 and 1.5 were acquired in fine-beam single (HH) co-polarization (FBS) and dual co- and cross-polarization (HH and HV) (FBD) modes, in an ascending orbit over an incidence angle range of 36.6° and 40.9°.

The images were acquired from three different sources as no single source captured annual and seasonal changes between 2009 and 2011: (1) PALSAR SLC (Single-Look Complex) Level 1.1 processed scenes were procured directly by JAXA; (2) PALSAR level 1.5 G processed scenes, which are Multi-Look Complex (MLC) and geo-referenced to UTM coordinates, were obtained through the K & C Initiative [48]; and (3) a mosaic with 25 m pixels was obtained freely from the JAXA website (http://www.eorc.jaxa.jp/ALOS/en/palsar_fnf/fnf_index.htm). PALSAR SLC Level 1.1 images were multi-look processed to 4-looks [49] corresponding to 12.5 m pixel spacing (~70 × 70 km area coverage) using the SARScape "image processing workbench" module within ENVI [50,51]. These were then speckle filtered using a Gamma MAP filter [52] with a 5 × 5-pixel window, radiometrically calibrated and normalized by eliminating incidence angle effects and antenna gain and spread loss patterns. The radiometric normalization process used a modified cosine model [53]. Terrain geocoding was then implemented using the SRTM 1-arcsec DEM, with the aid of the ALOS orbit data, and following the range-Doppler approach. Ortho images were projected to UTM coordinates (zone 36) using the

WGS84 reference ellipsoid and then assembled to image mosaic tiles geocoded to 30 m pixel size to match the Landsat images. Intensity values (amplitude) were subsequently converted to backscatter coefficients (σ^0) in decibels (dB) using Equation (1):

$$\sigma^0 = 10 \times Log_{10}[DN^2] + CF \tag{1}$$

where the Calibration Factor (CF) = -83, and DN is the digital number from each pixel location [54].

In summary, these processing sequences generated a mosaic of geo-coded, orthorectified, terrain-corrected, radiometrically calibrated and normalized PALSAR scenes with a pixel size of 30 m. Two sets of ortho-rectified images were used as reference images in geo-correction (image-to-image registration) of all other PALSAR images (see Dubeau [55] for details), including PALSAR Level 1.5 G images and the 25-m mosaics (Table 2). These PALSAR images provided about 70% coverage across the diagonal of the study area, leaving the upper-left and lower-right corners with no SAR data.

2.4. Variables Derived from the Landsat, PALSAR and DEM Data

Table 3 lists 19 vegetation, soil, and water indices that were derived from the Landsat 5 TM surface reflectance data and used in thematic classification. This is a small representative subset of the most widely used indices [12,56]. Another 18 morphometric terrain metrics were derived from the DEM to quantify the effects of topography and hydrological processes [28]. These metrics represented first and second order derivatives of the DEM (e.g., slope, aspect, gradient, and curvatures), and were combined to obtain secondary terrain attributes (e.g., terrain wetness index, terrain classification index in lowland, and terrain ruggedness index). All topographic metrics were calculated using the open source GIS SAGA (System for Automated Geoscientific Analyses, version 2.2.3) [57]. The predictor variables listed in Table 3 also include the coefficient of variation from a 3 × 3-pixel moving window applied to the HH and HV PALSAR images; it was used as a texture metric to evaluate how spatial heterogeneity in backscatter intensity can contribute to improving the discrimination of the wetland classes [58,59]. PALSAR L-band polarization intensity ratio HV/HH was selected for its effectiveness in discriminating flooded from non-flooded vegetation and water [47], while HH/HV demonstrated similar characteristics using SAR C-band data [60]. Full description of metrics with associated citations is given in [55]. For all variables in Table 3, various combinations of years and seasons (wet and dry) resulted in 103 total variables that were tested.

2.5. Image Classification

Mapping of wetlands and related ecosystems has greatly benefitted from the advance of machine learning ensemble classification, particularly the Random Forest (RF) classifier [15]. RF was selected for this study because it generally outperforms conventional classifiers such as the Gaussian maximum likelihood classifier [61,62], while performing favorably, or equally well, to other non-parametric approaches; e.g., CART [63,64], Support Vector Machines [32,65,66], Artificial Neural Networks [67], and K-Nearest Neighbor [68]. It is a powerful non-linear and non-parametric classifier that allows for fusion and aggregation of high- dimensional data from various sources (e.g., optical, SAR, and topography [30,69,70]; SAR and topography [21,58,71]; and optical and topography [72–74]). RF produces independently constructed classification trees, similar to the Classification and Regression (CART) method, using bootstrapped samples of the original data [75,76]. The outputs are combined in a voting procedure, which can generally improve accuracy over single classifications.

RF classifications were implemented using the R packages "randomForest" [76], "raster", and "rGDAL" [77] in R Statistics (R foundation for statistical Computing) from the R Development Core Team [78]. They were performed using different groups of satellite image sources (sensors), dates, and parameter combinations (Table 4). Topographic data were used in all classifications as they were regarded as invariant information over the period of the study.

Table 3. Vegetation, water, terrain indices, and SAR derived variables used in wetland classification.

Vegetation/Water Indices	Terrain Parameters/Indices
Normalized Difference Vegetation Index (NDVI)	Slope (radians)
Enhanced Vegetation Index (EVI)	Catchment slope (radians)
Soil Adjusted Vegetation Index (SAVI)	Slope height (m)
Modified Soil Adjusted Vegetation Index-2 (MSAVI2)	Length slope factor
Normalized Difference Moisture Index (NDMI)	Standardized height (m)
Normalized Burn Ratio (NBR)	Mid-Slope position (n-dimensional)
Normalized Burn Ratio-2 (NBR2)	Relative slope position
Modified Normalized Difference Water Index (MNDWI)	Topographic wetness index
Atmospheric Resistant Vegetation Index (ARVI)	SAGA Topographic wetness index
Soil and Atmospheric Resistant Vegetation Index (SARVI)	Terrain classification index for lowland (TCI$_{low}$)
Thiam's Transformed NDVI (TTVI)	Topographic position index
Global Environmental Monitoring Index (GEMI)	Morphometric protection index
Principal Component Transform (PC1)	Melton ruggedness number
PC2	Terrain ruggedness index
PC3	Terrain surface texture
Tasseled-cap Transformation (TC-Brightness)	Valley depth (m)
TC-Greenness (TCG)	Valley depth [relative height] (m)
TC-Wetness (TCW)	Vertical distance to channel network (m)
TCW-TCG	
PALSAR L-band derived variables	
SAR HH Texture (CV 3 × 3 window)	
SAR HV Texture (CV 3 × 3 window)	

In each tree generated by RF, 1/3 of the reference data (default value) were randomly set aside as an Out-of-Bag (OOB) sample for estimation of class prediction error [75]. The OOB errors for each tree were averaged over all trees [79]. OOB error was used as a basis for comparison of classifications to determine optimum input parameters, years and seasons (Table 4) as described below. OOB error has been shown to be optimistic compared to independent sample validation accuracy [75,80], but when applied consistently in the same manner, it can be an efficient way to compare classifications and conduct variable selection. It was preferred over independent validation for this study given: (1) the field generated reference data set sample size was limited due to poor accessibility to all parts of the wetlands; and (2) both the field and image-based reference samples follow the general arcuate shape of the wetlands and were probably spatially auto-correlated. Given the goal was to determine the geo-spatial data variables with the best potential for mapping these wetlands, it was decided to use all available reference data in the RF classifications for training and OOB bootstrapped error assessment.

The number of trees to grow (ntree) was determined by plotting OOB error against the number of trees for each land cover class using the full set of 103 predictor variables and 1125 reference samples. Overall, OOB error dropped rapidly from 50% to less than 5% (less than 1.5% for classes such as "Aquatic Bed" and "Forest") after the first 200 trees were grown; it then stabilized above 1000 trees. An ntree value of 5000 was selected for all subsequent classifications because there was negligible impact on run-time performance. To be efficient when large numbers of variables are used, a subset ($m_{try} = p^{0.5}$, where p is the number of variables [79], the algorithm default setting) was randomly selected at each node.

Error matrices were used as the primary means to compare class and overall accuracy, calculated as (100% − OOB error). Producer's accuracy (PA = 100% − errors of omission) and User's accuracy (UA = 100% − errors of commission) [81] are reported for each class. Overall accuracy is reported using predicted 95% confidence intervals [82]. In comparing two classifications, the McNemar test was used; it is based on the proportion of correct and incorrect pixels in a binary 2 × 2 contingency matrix [83,84].

Table 4. Overall accuracy for the RF classifications using various combinations of Landsat TM-5, derived SVIs, and PALSAR data. "Multi-source" includes all data variables as given in Table 3. Year and season are also noted. Topographic variables were included in all models since they are temporally invariant. OOB classification accuracy is given for wetland and upland separately, and overall (OA) ±95% confidence intervals (CI) of the mean.

RF Model	Landsat TM-5 [1]	PALSAR/L-Band [2]	No. of Variables	OOB Accuracy (%)		OA	
				Wetland	Upland	(%)	95% CIs
1. Multi-year–Bi-seasonal–Multi-source	2009 ^{w} + 2010 ^{d} + 2011 ^{w}	2009 ^{w} + 2010 ^{wd} + 2011 ^{d}	103	98.8	99.3	99.0	(97.6–100.0)
2. Multi-year–Bi-seasonal–Spectral	2009 ^{w} + 2010 ^{d} + 2011 ^{w}		83	97.4	99.3	98.1	(97.4–98.9)
3. Multi-year–Bi-seasonal–SAR		2009 ^{w} + 2010 ^{wd} + 2011 ^{d}	47	89.3	90.4	89.8	(88.0–91.5)
4. Single year–Dry Season–Multi-source	2010	2010	41	92.7	97.0	94.4	(93.7–95.0)
5. Multi-year–Wet Season–Multi-source	2009 + 2011	2009 + 2010	72	94.7	95.3	95.0	(94.4–95.6)
6. Multi-year–Wet Season–Spectral	2009 + 2011		62	92.1	94.6	93.1	(92.5–93.7)
7. Multi-year–Wet Season–SAR		2009 + 2010	28	85.2	89.5	86.9	(86.1–87.7)
8. Multi-year–Dry Season–Multi-source	2010	2010 + 2011	43	93.2	97.9	95.0	(94.4–95.6)
9. Single-year–Wet Season–Multi-source	2009	2009	45	91.5	95.1	92.9	(92.3–93.6)
10. Single-year–Wet Season–Spectral	2009		40	88.3	93.9	90.5	(89.9–91.2)
11. Single-year–Wet Season–Spectral	2011		40	88.1	86.7	87.5	(86.6–88.5)
12. Single year–Dry Season–Spectral	2010		39	92.7	95.6	93.8	(93.1–94.4)
13. Multi-year–Wet Season–Multi-source	2009	2010	45	91.3	94.4	92.6	(91.9–93.3)
14. Multi-year–Wet Season–Multi-source	2011	2010	45	91.5	90.4	91.1	(90.3–91.9)
15. Multi-year–Dry Season–SAR		2010 + 2011	22	85.5	86.5	85.9	(84.8–86.9)
16. Single-year–Wet Season–SAR		2009	23	83.9	87.2	85.2	(84.3–86.1)
17. Single-year–Wet Season–SAR		2010	23	83.6	79.5	82.0	(81.0–83.0)
18. Topographic (only)			18	75.7	64.8	71.4	(70.2–72.5)

Dry and wet seasons are denoted as "d" and "w" superscripts dw. [1] Landsat images: dry season, January 2010; wet season, November 2009 and October 2011; [2] M1-5 used PALSAR Level 1.1 and 1.5 images: dry season (HH), January 2010 and January 2011; wet season (HH and HV), July 2009 and July 2010. M6-17 used the PALSAR mosaic: wet season (HH and HV), July 2009 and July 2010 (October 2010 for eastern half of study area).

3. Results

Overall, the RF classifications produced consistent results with respect to depicting the spatial distribution of the main wetland classes. The Dabus wetlands can be divided into three main reaches/regions distributed along the stream elevation gradient, i.e., the upper/headwater, middle, and lower region (Figure 4). Each region presents distinct hydro-geomorphic, drainage, and soil characteristics that act as the determining factors controlling the wetland distribution and floristic composition. The Papyrus Swamp class covered much of the upstream area as well as small parts of the eastern lower region. Its northern boundaries were clearly defined against hillsides. As elevation rises gradually through the south, the Papyrus Swamps became more fragmented and formed a complex mosaic of habitats composed of Shrub Marshes and various herbaceous wetlands. The middle and lower regions comprised a wide marshland with diverse wetland classes; i.e., Emergent Marsh, Grass Marsh, interspersed with small stands of Papyrus and Shrub Marsh. The latter was rarely encountered during the field surveys but, in the classifications, its spatial distribution was closely associated with Papyrus Swamp. In the lower reaches, classes progressively transformed into a vast Wet Meadow that extended largely uninterrupted downstream to where the river basin narrows to a smaller valley before it returns to a faster flowing and more defined stream channel.

Forested Wetlands were generally found along margins between upland areas and floodplain ecotones, often as permanent riparian forests, which are relatively invariant to seasonal changes. The narrow floodplains found along the stream channels were mapped as Meadow Garden (MG). RF classifications detected most of the larger and clearly defined wetland areas that had been converted to agriculture. However, in many places, areas classified as Meadow Garden extended well beyond its expected range, especially for wet-season models.

3.1. Evaluation of Classification Models—Overall Accuracy

The overall wetland classification performance for the 18 RF model configurations (Table 4) is presented in order of their level of complexity, which was defined in terms of the number and diversity of input variables, as well as by the overall model prediction accuracy. All models include the 18 topographic variables as previously stated. A map produced from the best model (Model 1) is shown in Figure 4. Hereafter, models are referred to by their number (e.g., M1, M2, etc.).

Overall, OOB accuracy generally increased with the number of input variables. Combining data from multiple years and different data sources generally improved overall classification accuracy. However, the McNemar test showed that accuracies for the top four models (M1–M4), M7, and M8 were not significantly different ($p > 0.05$). Multispectral optical data outperformed SAR data in all RF models by 5–8%, e.g., M2 vs. M3, M6 vs. M7, and M10 vs. M16 or M17.

Overall accuracies were generally higher for dry season compared to wet season models. For example, M4 (dry season) overall accuracy was about 2% higher than wet season M9 ($p < 0.001$). This can be attributed to greater difficulty in detecting marsh classes such as Grass Marsh and Shrub Marsh in the wet season when they had full green vegetation cover with reflectance and backscatter that were similar to other vegetated classes. Dry season Landsat data and Landsat-derived spectral vegetation indices (SVIs) consistently contributed to overall OOB accuracies above 90% (M1, M2, M4, M8, and M12). Of the three single-year, single-source Landsat models (M10 (wet), 11 (wet), and 12 (dry)), M12 performed the best. These differences between dry and wet season results were diminished when multi-year and/or multi-source data were used. For example, both M5 (wet) and M8 (dry) achieved 95% overall accuracy. SAR-only models achieved lower accuracy overall as previously noted but there was negligible difference between dry and wet season SAR-based models results, e.g., 86.7% (M7—wet) and 85.9% (M15—dry). Overall classification accuracy for Terrestrial classes was slightly lower for the dry season model compared to the wet season (86% and 90%, respectively).
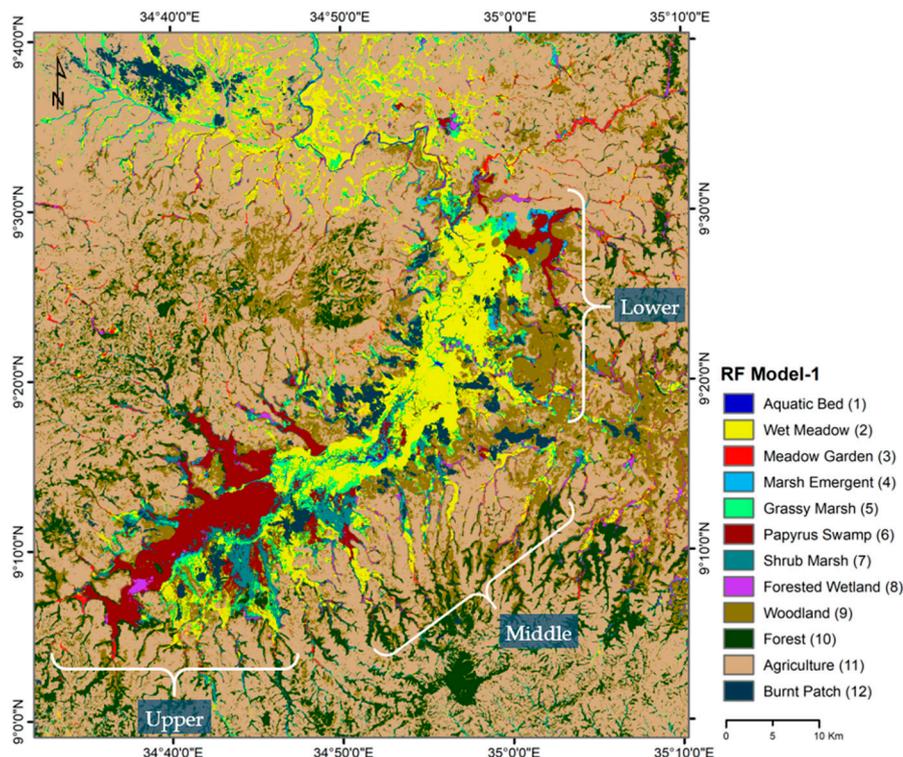
Figure 4. RF classification of the Dabus Wetlands using multi-year, bi-seasonal, and multi-source data (M1) with 103 predictor variables.

The seasonal differences in overall accuracy noted above were small but consistent. However, maps generated for each season were often quite similar. For example, cross tabulation of the two maps produced from single year multi-source dry (M4) and wet (M9) season models showed a high level of concordance, with only 2.1% of the pixels having different class assignments.

Analysis of Variable Contributions to Overall Classification Accuracy

RF overall accuracy was analyzed as a function of the number of model variables for a selection of nine models representing a range of input sources/variable combinations. Overall, OOB accuracy increased from 40% to 80–90% in three stages: (1) rapid model improvement occurred after the number of variables reached 5–8 for multi-source and optical-based models, and 9–10 for SAR based models; (2) for 8–20 variables, overall OOB accuracy increased to 75–80% for multi-source and optical models and 62–80% for SAR models; and (3) beyond 20 input variables performance continued to steadily improve. For multi-source and optical models, accuracy was greater than 90% with 30–35 variables and over 95–98% accuracy with 70–100 variables. For SAR models, the highest levels of accuracy of nearly 90% were achieved with more than 40 variables.

The variable importance rank score [85,86], expressed as a percentile, was used to evaluate the relative contributions of each predictor variable and season in the overall performance of the RF models. Among the variables with scores above the 75th percentile (Figure 5), Landsat short-wave infrared (b5 and b7) reflectance, which responds strongly to surface moisture [87,88], had overall scores consistently above the 84th and 87th percentiles, respectively. For the Landsat bands and their derived indices, overall variable importance scores for the dry season models were on average significantly higher than for the wet season models (79th vs. 46th percentile, respectively). Seasonal differences were also evident for individual bands. For example, green reflectance was more important in wet season than dry season models (80th vs. 33rd percentile, respectively), while red reflectance was more important in the dry season (93rd vs. 76th percentiles). Likewise, for SVIs, TCW and SAVI were more

important in the dry season (>95th percentile) than the wet season (<50th percentile). For the PALSAR variables, HV backscatter was among the most important variables in all RF models (>90th percentile), and above the 95th percentile for wet-season models. The six most important topographic variables, included in Figure 5 (bottom, right), were consistently ranked above the 70th percentile overall. Terrain Classification Index (TCI) performed the best, and was above the 91st percentile across all models.
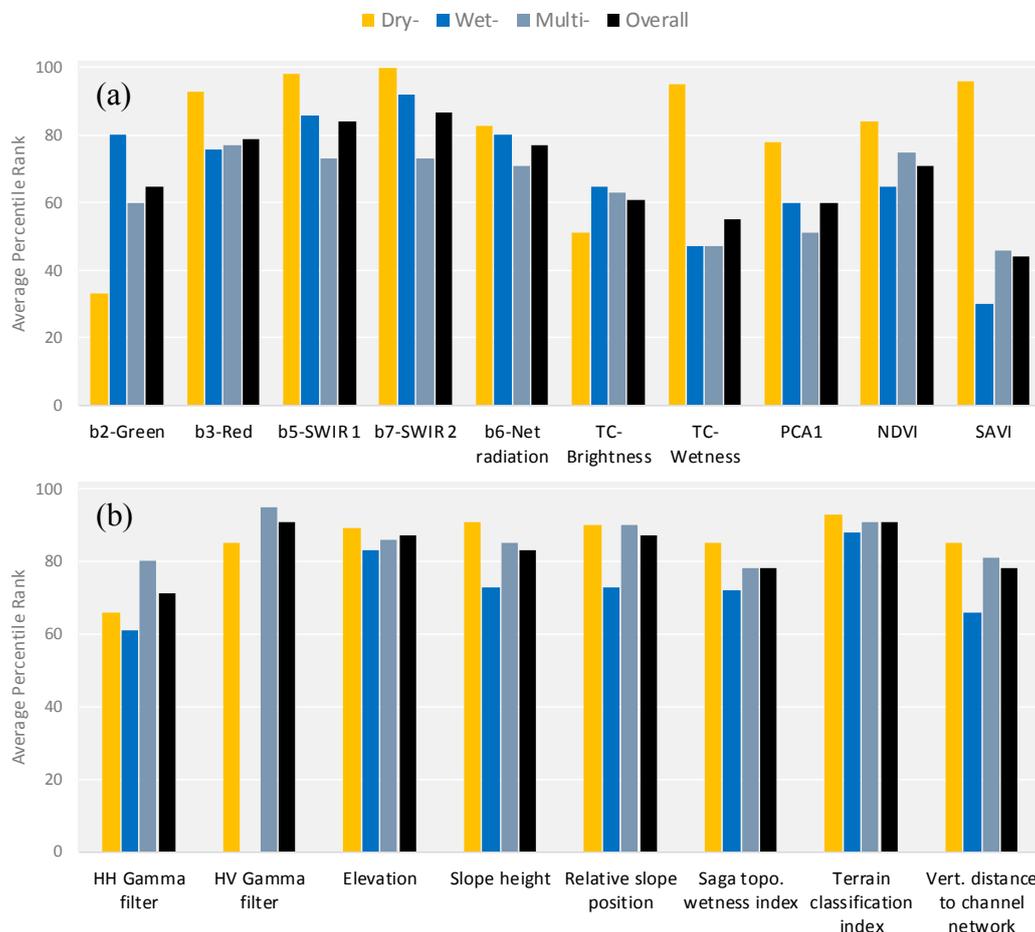

Figure 5. Average importance percentile rank scores for the most important variables; optical and SVIs (**a**), PALSAR HH and HV Gamma filter and six most important topographic variables (**b**).

3.2. Analysis of Individual Class Accuracies

Classification accuracy summary statistics (Table 5) were calculated from standard error matrices [81] that had been generated from the OOB samples for the first ten RF Models listed in Table 4. In general, terrestrial class accuracy was higher than wetland class accuracy and was more consistent across models. Confusion between wetland and terrestrial land cover classes was only about 1%, and generally limited to a few classes. For wetland classes, Aquatic Bed and Forested Wetland were the most accurate classes (98.3% and 96.0% average PA, respectively). Likewise, Wet Meadows achieved generally high accuracies despite being perhaps the most disturbed and impacted wetland class. The greatest source of confusion was among classes sharing similar plant community types, vegetation structure, and inundation regime, and confusion was greatest among the herbaceous classes (Grass Marsh, Marsh Emergent, and Garden Meadow). Grass Marsh ranked the lowest in the majority of models (PA and UA as low as 60.9% (M10) and 64.1% (M9), respectively). Marsh Emergent was second lowest while Garden Meadow was poorly predicted mostly in dry-season models (e.g., M2, M4, and M8). Shrub Marsh UA was among the lowest in M4, M8 (dry-season), M9, and M10 (wet-season).

Meadow Garden was generally confused with the Wet Meadow or Agriculture classes due to their spectral and spatial proximity. Adjacent successional classes, such as Shrub Marsh and Papyrus Swamp were also confused in places. Shrub Marsh was often observed along the landward margins of Papyrus Swamps. However, some of the largest patches appeared south of the main Papyrus stand. This area was poorly surveyed and accuracy was difficult to assess, particularly for Shrub Marsh. The area shows a high degree of fragmentation with several wetland classes distributed across the landscape without discernable ecological patterns. This phenomenon was not observed to the same extent elsewhere in the Dabus. Notably, this area was among the most remote and appeared to have been largely spared from anthropogenic disturbances and that may have allowed for the establishment of more diverse plant communities.

Table 5. User's and producer's accuracy (UA and PA, respectively; %) for M1-10 (Table 4), calculated using OOB samples. The lowest **UA** and **PA** for each model is highlighted in bold with shaded background.

RF Models:	M1		M2		M3		M4		M5	
Classes	UA	PA	UA	PA	UA	PA	UA	PA	UA	PA
1_Aquatic Bed	100.0	100.0	100.0	100.0	96.2	96.3	100.0	98.7	100.0	98.7
2_Wet Meadow	97.8	97.8	97.8	96.7	91.1	91.1	96.6	95.6	90.3	93.3
3_Meadow Garden	100.0	**95.5**	98.0	89.1	97.7	97.7	92.3	81.8	97.7	95.5
4_Marsh Emergent	**97.4**	100.0	94.8	96.1	82.7	88.2	91.9	89.5	80.4	97.4
5_Grass Marsh	96.8	95.3	95.5	98.4	83.6	71.9	83.1	92.2	97.9	73.4
6_Papyrus Swamp	98.0	100.0	96.0	98.0	86.0	92.9	90.2	92.9	95.1	97.0
7_Shrub Marsh	100.0	98.85	96.6	96.6	90.1	94.3	**88.0**	**83.9**	96.6	98.9
8_Forested Wetland	100.0	100.0	100.0	100.0	89.4	**84.4**	97.8	97.8	98.9	98.9
9_Woodland	99.3	98.03	100.0	98.0	87.8	85.5	95.4	96.1	94.1	94.7
10_Forest (mature)	100.0	100.0	100.0	100.0	87.5	86.8	97.5	98.4	99.1	94.2
11_Agriculture	98.7	100.0	97.5	100.0	94.9	96.2	96.8	96.8	96.8	96.8
12_Burned Patch	100.0	100.0	100.0	100.0	n/a	n/a	97.9	100.0	n/a	n/a
Overall Accuracy	99.0		98.1		89.8		94.4		95.0	
(%) (95% CIs)	(97.6–100.0)		(97.38–98.88)		(88.03–91.53)		(93.74–95.0)		(94.37–95.60)	
RF Models:	M6		M7		M8		M9		M10	
Classes	UA	PA	UA	PA	UA	PA	UA	PA	UA	PA
1_Aquatic Bed	100.0	98.7	93.7	94.9	100.0	98.7	100.0	98.7	100.0	98.7
2_Wet Meadow	**87.2**	91.1	85.4	84.4	94.5	95.6	90.3	93.3	87.0	88.9
3_Meadow Garden	93.7	**81.8**	88.5	83.6	92.1	79.5	100.0	90.9	91.5	**78.2**
4_Marsh Emergent	77.5	90.8	75.0	**78.9**	94.7	93.4	79.1	**89.5**	75.3	88.2
5_Grass Marsh	92.4	76.6	75.4	67.2	83.8	89.1	87.2	64.1	86.7	60.9
6_Papyrus Swamp	92.1	93.9	82.9	87.9	92.2	96.0	88.7	94.9	85.6	89.9
7_Shrub Marsh	92.3	96.5	84.0	90.8	**87.9**	**83.9**	86.5	95.4	81.8	93.1
8_Forested Wetland	99.0	99.0	88.7	87.8	97.8	97.8	100.0	96.9	100.0	96.9
9_Woodland	92.4	95.4	86.8	86.8	96.7	97.4	93.4	92.8	90.3	92.1
10_Forest (mature)	99.1	94.2	92.2	88.4	97.5	98.3	99.1	95.9	98.3	95.9
11_Agriculture	96.1	94.2	93.5	92.9	98.1	98.1	95.6	96.8	94.8	94.2
12_Burned Patch	n/a	n/a	n/a	n/a	97.8	100.0	n/a	n/a	n/a	n/a
Overall Accuracy	93.1		86.9		95.0		92.9		90.5	
(%) (95% CIs)	(92.51–93.74)		(86.11–87.68)		(94.36–95.65)		(92.30–93.57)		(89.87–91.17)	

While differences between M1 and M2 were negligible (accuracy difference <1%; cross tabulation pixel assignment differences <4%), by contrast, M3 (SAR) overall accuracy was significantly lower and map cross-tabulation between M1 and M3 and between M2 and M3 showed differences in class assignments for 31.6% and 32.9% of the pixels, respectively. The main classes with lower PA and UA for all three models were Grass Marsh and Marsh Emergent. For M3, however, Shrub Marsh was also confused with the largest number of classes (n = 7), while classes with dense canopy cover such as

Papyrus Swamp, Forested Wetland, and Forest, were more confused. Meadow Garden was the only class that achieved higher accuracy (PA) using M3 compared to M1 and M2.

Seasonal Differences in Individual Class Accuracies

Analysis of individual class accuracy for the dry and wet seasons was carried out using M4 and M9, and M7 and M15, for comparison of results for multi-source and SAR based model configurations, respectively. Overall accuracy of terrestrial classes (96–97%) did not change between the dry and wet seasons. However, some wetland classes showed marked differences between seasons; e.g., Grass Marsh (PA = 92.2% (M4) and 64.1% (M9)), and Marsh Emergent (UA = 91.9% (M4) and 79.1% (M9)), as shown in Table 5. The poorest dry season wetland classes were Meadow Garden (PA = 89.1%) and Shrub Marsh (PA = 83.9%). For the wet season model M9, Grass Marsh and Marsh Emergent accounted for more than 40% of all confusion among pixels. PA for Grass Marsh was only 64.1%, as many pixels were mis-classified as Marsh Emergent, Wet Meadow, and Shrub Marsh. Commission errors for Marsh Emergent also included Papyrus Swamp and Wet Meadow, among others.

For SAR-based wet and dry season models (M7 and M15, respectively), the lowest accuracy was for Grass Marsh and Marsh Emergent, both with PA and UA less than 79% for the dry and wet season models. M7 poorly predicted Forested Wetland (PA = 78.9%) and Shrub Marsh (UA = 80.4%), the latter being confused with seven of the 11 classes. Other commonly confused class pairs included: Forested Wetland and Woodland; Woodland and Forest; and Woodland and Agriculture. Aggregating Marsh Emergent and Grass Marsh into a Herbaceous Marsh class produced less than 2% gain in overall accuracy, while aggregating the three marsh classes, Emergent, Grass, and Shrub, into one Marsh class, produced a 4% gain in overall accuracy (75.5–79.5%).

3.3. Analysis of Differences in Class Extent between RF Models

For comparative analysis, the spatial extent of wetland and terrestrial classes was estimated for a subset of the RF models, including: M1 as the best but most complex model; M4 vs. M9 and M7 vs. M15, which show seasonal differences and optical vs. SAR differences, respectively; and M12, which was selected as the "best" model with the least number of spectral variables (see Table 4 for descriptions of each model).

Figure 6 shows that wetland classes represented about 25–27% of the total land area. Within the wetland classes, Wet Meadow and Papyrus Swamp accounted for 37–41% and 19–21% of the total area, respectively, while Shrub Marsh covered 12–18%. Together these three classes represented 69–80% of the total wetland area. Wet Meadow and Papyrus Swamp area remained consistent for most multi-source models. Aquatic Bed covered about 0.5% of the total wetland area and exhibited high variance across models. The extent of terrestrial/upland classes was generally consistent across models M4, M9, and M12. Overall, Agriculture represented 63–68% of the total terrestrial land area. The remaining non-cultivated area was comprised of woodlands (21–27%) and sparsely distributed patches of forest (9–20%). The dry-season SAR-based model, M15, estimated Forest coverage to be about double that of the other models.
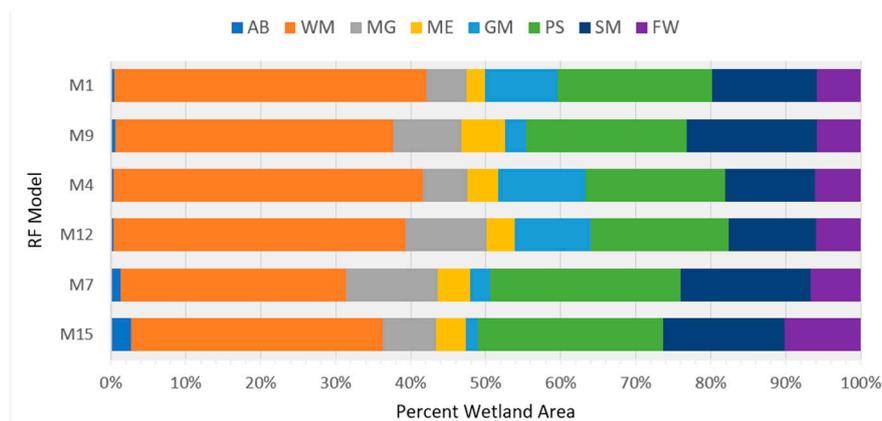
Figure 6. Percentage of wetland area by wetland class for selected RF models. For M1, M4, and M12, Burn Patch areas were attributed to wetland classes based on wet-season model classifications.

4. Discussion

4.1. Interpretation of Main Findings and Relations to Previous Studies

Overall, Random Forest classification produced consistent results with respect to mapping the Dabus wetlands, as well as the surrounding terrestrial land covers. The RF models evaluated using various combination of multi-source and multi-date model configurations were generally accurate in predicting the distribution of wetland classes. The RF maps show the well-defined arcuate shape of the Dabus wetlands, which is emphasized by the surrounding terrestrial landscape with its sparsely vegetated rolling hillsides.

The two main wetland ecosystems were well mapped, namely Papyrus Swamps, extending across most of the upper wetland region, and herbaceous marshes and meadows, stretching downstream from where the main stand of Papyrus ends. Individual class accuracies varied according to the ecology of the dominant species, phenology, and disturbance, which in turn affect reflectance and backscatter characteristics [89]. Perennial wetlands such as Papyrus Swamps and Forested Wetlands, which occur as homogenous plant communities, generally achieved higher accuracies and consistency (stability) between classification models compared to seasonally inundated herbaceous wetlands. Shrub Marsh was poorly classified across all models in part due to its highly scattered spatial distribution and because it was a class difficult to survey in the field. By comparison, herbaceous wetlands, which spread over large extents in seasonally inundated areas, cycle through extreme conditions from flooded marshland more than a meter deep to a barren landscape following intense grazing and burning. However, one of these classes, Wet Meadow achieved relatively high accuracy despite experiencing extreme changing conditions. Wet Meadow is relatively homogeneous due to the dominance of mixed C_4 tall and short grasses in the plant communities, with additional C_3 species and aquatic macrophytes. A high level of disturbance, such as grazing and fire is generally associated with increased abundance of C_4 species [90,91].

Random Forest Classifier Performance and Variable Importance

Random Forest classifications performed well, confirming the widely reported effectiveness of the RF algorithm for land cover classification (e.g., [15,58,64,65]), and particularly for mapping wetlands in tropical environments (e.g., [73,89,92]). Overall, OOB accuracy was above 80% for most models, above 90% for a selection of optimized models, and as high as 99% for model M1, which integrated spectral, SAR and topographic data, and images from multiple years and seasons. Improvement was more significant when optical variables were added to SAR based models (9%) than vice versa (1–2%).

The integration of multi-source data to improve RF model performance has been reported in several studies in tropical environments [30,93,94]. Optical and SAR imagery provide complementary

information and are often used in combination, while addition of topographic variables has also been shown to improve wetland and other land cover classification [15,21,95,96]. This was confirmed in this study as variable importance analysis showed that shortwave-infrared reflectance (Landsat bands 5 and 7), PALSAR HV backscatter and several topographic variables (terrain classification index, relative slope position, elevation, and slope height, in order of importance) contributed most to overall classification accuracy. Other variables such as Landsat-green, TCW, and SAVI were important but only for one season. SWIR variables contributed to improving classification across all classes. The contributions of Landsat band 5 were generally greater for Forested Wetland, while band 7's response was markedly stronger for Papyrus Swamp and Wet Meadow, but only for dry season imagery. The strong SWIR response for these two classes is attributable to the sensitivity of SWIR reflectance to soil moisture absorption and surface texture [88]. The inclusion of SAR data had a relatively limited impact overall on the importance ranking of optical variables, although PALSAR HV outranked most variables when used in combination with optical variables. Corcoran, Knight and Gallant [95] discriminated upland, water, and wetland areas using RF with a similar assortment of predictors (e.g., Landsat 5 TM NIR and SWIR, elevation and curvature, hydric soils data, as well as PALSAR (L-band) cross-polarization (HV) data). Other studies have confirmed the importance of NDVI [14], NDMWI [97], Tasseled-cap components [98,99], and Landsat thermal band 6 as wetland predictors [95,98]. Notably, "Net Radiation", derived from Landsat band-6 (thermal), was among the top five optical variables for this study, and class response was consistent across RF models.

The SAR-based models evaluated in this study yielded overall OOB accuracy ranging between 82.0% and 85.2% for single-year models and between 86.9% and 89.7% for multi-year models. The contribution of PALSAR L-band HH and HV data to wetland classification has been well documented [33,34,58,100]. For example, large-area mapping of the Pantanal using PALSAR L-band FBD [33], achieved 80% accuracy across the entire area. The importance of cross-polarization (HV) backscatter was consistently higher than HH for all RF models. In a review paper, Henderson and Lewis [18] noted that in a number of studies HV provided better results than HH for wetland mapping. More specifically, in this study wet-season HV backscatter was an important predictor for all land cover classes, but HH was generally more important in distinguishing wetland classes than terrestrial classes. For example, the HV contribution to detecting upland Forest, a characteristically strong "volume-scatterer", was markedly higher than HH (wet-season data). Papyrus Swamp was well classified because its HH and HV backscatter was intermediate in between forest wetland/upland classes and the lower backscatter of herbaceous and shrub dominated classes. Bourgeau-Chavez et al. [101] reported similar backscatter responses in multi-seasonal data for Phragmites, a tall reed exhibiting similar structural characteristics as Papyrus.

The relatively poor classification performance achieved by SAR-based models, compared to optical models, could also have been partly attributable to the use of fewer predictor variables for the SAR models, mainly HH and HV backscatter intensity. Addition of phase information may improve wetland classification [102,103], while fully polarimetric data allow an array of polarimetric decomposition techniques that have been successfully used for characterization and classification of wetlands [60,104]. In addition, interferometric data can provide improved topographic information or vegetation surface model data that could improve classifications.

Use of multi-source (optical, radar, and topography), multi-year, and wet and dry season data is recommended to achieve the highest accuracies, as was shown for M1. Besides one-time mapping, however, low error levels are required for temporal monitoring because classification error in either or both maps impacts temporal change metrics when two maps are cross-tabulated. The M1 99% overall accuracy and 95.3% minimum class accuracy are probably sufficient for monitoring on a five-year cycle (given M1 had data from three different years). However, many of the other models were not deemed to be sufficiently accurate for temporal analysis. For example, comparing M9 and M4 (2009 wet- and 2010 dry-season optical-topo models, respectively, but only two months apart) showed that estimated wet season wetland extent (M9) was 7.2% larger than dry season (M4) extent, while

upland/terrestrial areas increased by 2.6%. These overall changes are relatively small and within the range of classification error levels for each model (7.1% and 5.5% average error for M9 and M4, respectively). Most changes in class assignments between M9 and M4 were also in class boundary areas where errors are expected to be higher. However, in some areas, seasonal changes were significantly greater than these error levels. For example, near the middle reach of the Dabus wetlands Grass Marsh dominated during the dry season and changed to Emergent Marsh during the wet season, as was expected for this ecological setting. Such differences are likely due to a mix of real change and map error propagation. Full temporal change analysis using such maps should therefore incorporate error statistics to estimate the confidence that detected change is real and from that the range of the possible areal extent of such change.

4.2. Limitations and Recommendations for Future Mapping of Wetlands

Results obtained in this study were within the range of wetland classification accuracies previously published, yet such high accuracy levels raise the question of the potential for overfitting the classifier, as overfitting can limit the potential for generalization [105]. Although RF is generally considered robust to overfitting [106], it is highly likely that overall classification accuracy levels reported in this study were overly optimistic since the RF accuracy assessment was obtained from the "Out-of-Bag" (OOB) accuracy estimate, which is known to represent inflated accuracy [75,80]. OOB accuracy is useful for comparison of multiple classification models as in this study but independent validation is required to determine absolute accuracy.

This study was also limited by the quality of the field reference data that could be collected in this remote area. Gathering representative reference data with limited prior knowledge of the types of wetlands and their distribution can be a challenge. The reference data set was carefully evaluated, through visual inspection, and by using separability analysis [55] to assist with eliminating outliers/misclassified locations. RF classifications based on imbalanced training data can lead to over-prediction of the classes with the most training samples [107]. To limit the effects of using imbalanced datasets on RF predictions, effort was made to acquire a relatively equal number of reference points across most classes (Table 1), or at the very least, proportional to the class representation in the wetland, although information on class proportions was not available prior to conducting the classifications. In addition, as a result of the Dabus Marsh arcuate configuration in the landscape, the spatial distribution of the reference data shows a highly-clustered pattern with expected spatial autocorrelation, which was not measured. Such clustering of reference sample locations can contribute to classification accuracy inflation [80,108]; however, this could not be avoided. Finally, the field surveys represented less than 5–10% of the total area, and were mainly concentrated in the northwestern portion of the Dabus Wetlands. The likelihood of having missed important class examples is significant and may explain why some areas yielded much lower class-membership probabilities compared to the areas with abundant reference samples.

5. Conclusions

Ensemble-learning classifiers, such as Random Forest, present promising results for mapping wetland ecosystems in tropical environments. Spectral (Landsat-5 TM) and SAR (PALSAR L-band) data used in combination with topographic indices derived from an SRTM 30 m DEM provided the best classification performance of the Dabus Wetlands. Spectral and topographic data performed nearly as well without SAR data, while accuracies using only SAR with topographic data were 6–8% lower overall. SAR performance remained acceptable (82–89%), particularly given it can be acquired under cloudy conditions typical of tropical regions. Dry season data performed slightly better than wet season data and higher accuracies were achieved when they were combined.

The resulting thematic maps showed the extent and location of eight Dabus wetland classes. They were largely dominated by seasonally inundated grass meadows mixed with patches of floristically rich sedge marsh found within broad depressions and associated with the various stream channels.

The Papyrus Swamp formed the second largest area of wetlands extending across a wide expanse of the upper reaches of the Dabus Wetlands. It plays an important role in the water balance, as it acts as a reservoir, slowly releasing water that benefits downstream areas used by farmers.

The approach followed in this study demonstrated the potential of using multi-sensor and topographic data with the Random Forest classifier for classification of a large and relatively remote wetland that had not been mapped extensively in the past. The results provide information on data sources, variables and seasons that will aid development of monitoring and management of this and other similar tropical wetlands.

Author Contributions: Pierre Dubeau developed the original research concept and field survey plan, with the assistance of Dikaso Gojamme Unbushe and Lisa-Maria Rebelo. Douglas J. King advised on the research design, implementation, and analysis as the academic supervisor. Pierre Dubeau wrote the R scripts (adapted from a script provided by Millard and Richardson]) and analyzed the results. Pierre Dubeau wrote the first drafts of the paper and Douglas J. King contributed the main edits and advice on the content. Dikaso Gojamme Unbushe and Lisa-Maria Rebelo provided additional edits and inputs to the content.

Conflicts of Interest: The authors declare no conflict of interest.

References

1. Mitsch, W.J.; Gosselink, J.G. *Wetlands*, 4th ed.; John Wiley & Sons: New York, NY, USA, 2007; p. 582. ISBN 978-0-471-69967-5.
2. Chapman, L.J.; Balirwa, J.; Bugenyi, F.W.B.; Chapman, C.A.; Crisman, T.L. Wetlands of East Africa: Biodiversity, exploitation, and policy perspectives. In *Biodiversity in Wetland: Assessment, Function and Conservation*; Gopal, B., Junk, W.J., Davis, J.A., Eds.; Backhuys Publishers: Leiden, The Netherlands, 2001; Volume 2, pp. 101–131.
3. Hughes, R.H.; Hughes, J.S. *A Directory of African Wetlands*; IUCN—The World Conservation Union: Gland, Switzerland; Cambridge, UK; United Nations Environment Programme: Nairobi, Kenya; World Conservation Monitoring Centre: Cambridge, UK, 1992; p. 819. ISBN 978-2880329495.
4. Jones, M.B. The photosynthetic characteristics of papyrus in a tropical swamp. *Oecologia* **1987**, *71*, 355–359. [CrossRef] [PubMed]
5. Betbeder, J.; Gond, V.; Frappart, F.; Baghdadi, N.N.; Briant, G.; Bartholome, E. Mapping of Central Africa forested wetlands using remote sensing. *IEEE J. Sel. Top. Appl. Earth Obs. Remote Sens.* **2014**, *7*, 531–542. [CrossRef]
6. Finlayson, C.M.; Davidson, N.C.; Spiers, A.G.; Stevenson, N.J. Global wetland inventory–current status and future priorities. *Mar. Freshw. Res.* **1999**, *50*, 717–727. [CrossRef]
7. McCartney, M.; de Silva, S.; Rebelo, L.-M.; Greatrix, E.; Mapedza, E.; Morardet, S.; Murgue, C.; Noble, A. *Wetlands and People*; IWMI International Water Management Institute: Colombo, Sri Lanka, 2014; p. 32. ISBN 978-92-9090-784-8.
8. Coughanowr, C. *Wetlands of the Humid Tropics: Water Related Issues and Problems of the Humid Tropic and Other Warm Humid Regions*; UNESCO: Paris, France, 1998; p. 47.
9. Finlayson, C.M.; D'Cruz, R.; Aladin, N.; Barker, D.; Beltram, G.; Brouwer, J.; Davidson, N.; Duker, L.; Junk, W.; Kaplowitz, M. Inland water systems. In *Ecosystems and Human Well-Being: Current State and Trends*; Hassan, R., Scholes, R.J., Ash, N., Eds.; Island Press: Washington, DC, USA, 2005; Volume 1, pp. 553–583.
10. Environment Protection Authority (EPA). *National Report on the 43 Surveyed Wetlands*; The Ecosystem Department of the Environment Protection Authority (EPA): Addis Ababa, Ethiopia, 2003; p. 122.

11.　Geheb, K.; Yilma, D.A. *Wetlands of Ethiopia: Proceedings of a Seminar on the Resources and Status of Ethiopia's Wetlands*; Abebe, Y.D., Geheb, K., Eds.; IUCN—The World Conservation Union: Addis Ababa, Ethiopia, 2003; p. 116.

12.　Ozesmi, S.L.; Bauer, M.E. Satellite remote sensing of wetlands. *Wetl. Ecol. Manag.* **2002**, *10*, 381–402. [CrossRef]

13.　Rosenqvist, A.; Shimada, M.; Milne, A.K. The ALOS Kyoto & Carbon Initiative. In Proceedings of the International Geoscience and Remote Sensing Symposium (IGARSS 2007), Barcelona, Spain, 23–28 July 2007; IEEE: Barcelona, Spain, 2007; pp. 3614–3617.

14.　Adam, E.; Mutanga, O.; Rugege, D. Multispectral and hyperspectral remote sensing for identification and mapping of wetland vegetation: A review. *Wetl. Ecol. Manag.* **2010**, *18*, 281–296. [CrossRef]

15.　Belgiu, M.; Drăguţ, L. Random Forest in remote sensing: A review of applications and future directions. *ISPRS J. Photogramm. Remote Sens.* **2016**, *114*, 24–31. [CrossRef]

16.　Dingle Robertson, L.; King, D.J.; Davies, C. Object-based image analysis of optical and radar variables for wetland evaluation. *Int. J. Remote Sens.* **2015**, *36*, 5811–5841. [CrossRef]

17.　Dingle Robertson, L.; King, D.J.; Davies, C. Assessing land cover change and anthropogenic disturbance in wetlands using vegetation fractions derived from Landsat 5 TM imagery (1984–2010). *Wetlands* **2015**, *35*, 1077–1091. [CrossRef]

18.　Henderson, F.M.; Lewis, A.J. Radar detection of wetland ecosystems: A review. *Int. J. Remote Sens.* **2008**, *29*, 5809–5835. [CrossRef]

19.　Jones, K.; Lanthier, Y.; van der Voet, P.; van Valkengoed, E.; Taylor, D.; Fernández-Prieto, D. Monitoring and assessment of wetlands using Earth Observation: The GlobWetland project. *J. Environ. Manag.* **2009**, *90*, 2154–2169. [CrossRef] [PubMed]

20.　Klemas, V. Remote sensing of emergent and submerged wetlands: An overview. *Int. J. Remote Sens.* **2013**, *34*, 6286–6320. [CrossRef]

21.　Millard, K.; Richardson, M. Wetland mapping with LiDAR derivatives, SAR polarimetric decompositions, and LiDAR–SAR fusion using a Random Forest classifier. *Can. J. Remote Sens.* **2013**, *39*, 290–307. [CrossRef]

22.　Wolf, B. GlobWetland II: Wetland mapping in North Africa. In Proceedings of the 2011 GEOSS Workshop XLI, Vancouver, BC, Canada, 24 July 2011; pp. 1–40.

23.　Jensen, J.R. *Remote Sensing of the Environment: An Earth Resource Perspective*, 2nd ed.; Pearson Prentice Hall: Upper Saddle River, NJ, USA, 2007; p. 592. ISBN 978-0131889507.

24.　Kumar, L.; Schmidt, K.; Dury, S.; Skidmore, A. Review of hyperspectral remote sensing and vegetation science. In *Imaging Spectrometry: Basic Principles and Prospective Applications*; van der Meer, F.D., de Jong, S.M., Eds.; Kluwer Academic: Dordrecht, The Netherlands, 2001; Volume 4, pp. 111–155.

25.　Silva, T.S.F.; Costa, M.P.F.; Melack, J.M. Spatial and temporal variability of macrophyte cover and productivity in the eastern Amazon floodplain: A remote sensing approach. *Remote Sens. Environ.* **2010**, *114*, 1998–2010. [CrossRef]

26.　Töyrä, J.; Pietroniro, A. Towards operational monitoring of a northern wetland using geomatics-based techniques. *Remote Sens. Environ.* **2005**, *97*, 174–191. [CrossRef]

27.　Ouchi, K. Recent trend and advance of Synthetic Aperture Radar with selected topics. *Remote Sens.* **2013**, *5*, 716–807. [CrossRef]

28.　Hengl, T.; Reuter, H.I. *Geomorphometry: Concepts, Software, Applications*; Elsevier Scientific Publishing: Oxford, UK, 2009; p. 765. ISBN 978-0-12374345-9.

29.　Wilson, J.P.; Gallant, J.C. Digital terrain analysis. In *Terrain Analysis: Principles and Applications*; Wilson, J.P., Gallant, J.C., Eds.; John Wiley and Sons: New York, NY, USA, 2000; pp. 87–131.

30.　Bwangoy, J.-R.B.; Hansen, M.C.; Roy, D.P.; Grandi, G.D.; Justice, C.O. Wetland mapping in the Congo Basin using optical and radar remotely sensed data and derived topographical indices. *Remote Sens. Environ.* **2010**, *114*, 73–86. [CrossRef]

31.　Adam, E.; Mutanga, O.; Abdel-Rahman, E.M.; Ismail, R. Estimating standing biomass in papyrus (*Cyperus papyrus* L.) swamp: Exploratory of In Situ hyperspectral indices and random forest regression. *Int. J. Remote Sens.* **2014**, *35*, 693–714. [CrossRef]

32.　Adam, E.; Mutanga, O.; Odindi, J.; Abdel-Rahman, E.M. Land-use/cover classification in a heterogeneous coastal landscape using RapidEye imagery: Evaluating the performance of Random Forest and Support Vector Machines classifiers. *Int. J. Remote Sens.* **2014**, *35*, 3440–3458. [CrossRef]

33. Evans, T.L.; Costa, M.; Tomas, W.M.; Camilo, A.R. Large-scale habitat mapping of the Brazilian Pantanal wetland: A synthetic aperture radar approach. *Remote Sens. Environ.* **2014**, *155*, 89–108. [CrossRef]

34. Hess, L.L.; Melack, J.M.; Affonso, A.G.; Barbosa, C.; Gastil-Buhl, M.; Novo, E.M.L.M. Wetlands of the Lowland Amazon Basin: Extent, vegetative cover, and dual-season inundated area as mapped with JERS-1 Synthetic Aperture Radar. *Wetlands* **2015**, *35*, 745–756. [CrossRef]

35. Tilahun, S.; Edwards, S.; Egziabher, T.B.G. *Important Bird Areas of Ethiopia: A First Inventory*; Ethiopian Wildlife and Natural History Society: Addis Ababa, Ethiopia, 1996; p. 300.

36. Gamachu, D. *Aspects of Climate and Water Budget in Ethiopia*; Addis Ababa University Press: Addis Ababa, Ethiopia, 1977; p. 49.

37. Ethiopian Meteorological Service Agency (EMSA). Available online: https://www.ethiomet.gov.et/ (accessed on 30 September 2016).

38. Muthuri, F.M.; Jones, M.B. Nutrient distribution in a papyrus swamp: Lake Naivasha, Kenya. *Aquat. Bot.* **1997**, *56*, 35–50. [CrossRef]

39. IUCN—The World Conservation Union. 2016-1 IUCN Red List of Threatened Species, (Version 2.1). Available online: http://www.iucnredlist.org (accessed on 4 March 2016).

40. Dixon, A.B.; Wood, A.P. Wetland cultivation and hydrological management in eastern Africa: Matching community and hydrological needs through sustainable wetland use. *Nat. Resour. Forum* **2003**, *27*, 117–129. [CrossRef]

41. Spasojevic, M.J.; Aicher, R.J.; Koch, G.R.; Marquardt, E.S.; Mirotchnick, N.; Troxler, T.G.; Collins, S.L. Fire and grazing in a mesic tallgrass prairie: Impacts on plant species and functional traits. *Ecology* **2010**, *91*, 1651–1659. [CrossRef] [PubMed]

42. Cowardin, L.M.; Carter, V.; Golet, F.C.; LaRoe, E.T. *Classification of Wetlands and Deepwater Habitats of the United States*; FWS/OBS-79/31; USDI Fish and Wildlife Service: Washington, DC, USA, 1979; p. 103.

43. Farr, T.G.; Rosen, P.A.; Caro, E.; Crippen, R.; Duren, R.; Hensley, S.; Kobrick, M.; Paller, M.; Rodriguez, E.; Roth, L.; et al. The shuttle radar topography mission. *Rev. Geophys.* **2007**, *45*, RG2004. [CrossRef]

44. Chander, G.; Markham, B.L.; Barsi, J.A. Revised Landsat-5 Thematic Mapper radiometric calibration. *IEEE Geosci. Remote Sens. Lett.* **2007**, *4*, 490–494. [CrossRef]

45. Zhu, Z.; Woodcock, C.E. Object-based cloud and cloud shadow detection in Landsat imagery. *Remote Sens. Environ.* **2012**, *118*, 83–94. [CrossRef]

46. Richter, R.; Schläpfer, D.; Müller, A. An automatic atmospheric correction algorithm for visible/NIR imagery. *Int. J. Remote Sens.* **2006**, *27*, 2077–2085. [CrossRef]

47. De Grandi, G.D.; Bouvet, A.; Lucas, R.M.; Shimada, M.; Monaco, S.; Rosenqvist, A. The K & C PALSAR mosaic of the African continent: Processing issues and first thematic results. *IEEE Trans. Geosci. Remote Sens.* **2011**, *49*, 3593–3610. [CrossRef]

48. Rebelo, L.M. Mapping inland wetlands in Africa using long waveband radar: The ALOS Kyoto and Carbon Initiative. In Proceedings of the WaterNet/WARFSA/GWP-SA Symposium, Entebbe, Uganda, 28–30 October 2009; pp. 1–7.

49. Bruniquel, J.; Lopes, A. Multi-variate optimal speckle reduction in SAR imagery. *Int. J. Remote Sens.* **1997**, *18*, 603–627. [CrossRef]

50. ITT Visual Information Solutions. *The Environment for Visualizing Images ENVI Version 5.0 and SARScape Version 5.1*; ITT Visual Information Solutions: Boulder, CO, USA, 2012; p. 64.

51. Sarmap SA. *Synthetic Aperture Radar and SARscape: SAR-Guidebook*; Sarmap SA: Purasca, Switzerland, 2009; p. 274.

52. Lopes, A.; Nezry, E.; Touzi, R.; Laur, H. Structure detection and statistical adaptive speckle filtering in SAR images. *Int. J. Remote Sens.* **1993**, *14*, 1735–1758. [CrossRef]

53. Ulaby, F.T.; Dobson, M.C. *Handbook of Radar Scattering Statistics for Terrain*; Artech House, Inc.: Norwood, MA, USA, 1989; p. 357. ISBN 978-0-89006-336-1.

54. Rosenqvist, A.; Shimada, M.; Ito, N.; Watanabe, M. ALOS PALSAR: A pathfinder mission for global-scale monitoring of the environment. *IEEE Trans. Geosci. Remote Sens.* **2007**, *45*, 3307–3316. [CrossRef]

55. Dubeau, P. Mapping and Characterizing Wetlands and Wetland Dynamics in the Highlands of Ethiopia Using Random Forest Classification. Master's Thesis, Carleton University, Ottawa, ON, Canada, 2016.

56. Bannari, A.; Morin, D.; Huete, A.R.; Bonn, F. A review of vegetation indices. *Remote Sens. Rev.* **1995**, *13*, 95–120. [CrossRef]

57. Conrad, O.; Bechtel, B.; Bock, M.; Dietrich, H.; Fischer, E.; Gerlitz, L.; Wehberg, J.; Wichmann, V.; Böhner, J. System for automated geoscientific analyses (SAGA) v. 2.1.4. *Geosci. Model Dev.* **2015**, *8*, 1991–2007. [CrossRef]

58. Clewley, D.; Whitcomb, J.; Moghaddam, M.; McDonald, K.; Chapman, B.; Bunting, P. Evaluation of ALOS PALSAR data for High-Resolution mapping of vegetated wetlands in Alaska. *Remote Sens.* **2015**, *7*, 7272–7297. [CrossRef]

59. Simard, M.; Saatchi, S.S.; De Grandi, G.D. The use of decision tree and multiscale texture for classification of JERS-1 SAR data over tropical forest. *IEEE Trans. Geosci. Remote Sens.* **2000**, *38*, 2310–2321. [CrossRef]

60. Brisco, B.; Kapfer, M.; Hirose, T.; Tedford, B.; Liu, J. Evaluation of C-band polarization diversity and polarimetry for wetland mapping. *Can. J. Remote Sens.* **2011**, *37*, 82–92. [CrossRef]

61. Rodriguez-Galiano, V.F.; Ghimire, B.; Rogan, J.; Chica-Olmo, M.; Rigol-Sanchez, J.P. An assessment of the effectiveness of a Random Forest classifier for land-cover classification. *ISPRS J. Photogramm. Remote Sens.* **2012**, *67*, 93–104. [CrossRef]

62. Waske, B.; Braun, M. Classifier ensembles for land cover mapping using multitemporal SAR imagery. *ISPRS J. Photogramm. Remote Sens.* **2009**, *64*, 450–457. [CrossRef]

63. Gislason, P.O.; Benediktsson, J.A.; Sveinsson, J.R. Random Forests for land cover classification. *Pattern Recog. Lett.* **2006**, *27*, 294–300. [CrossRef]

64. Sonobe, R.; Tani, H.; Wang, X.; Kobayashi, N.; Shimamura, H. Parameter tuning in the Support Vector Machine and Random Forest and their performances in cross- and same-year crop classification using TerraSAR-X. *Int. J. Remote Sens.* **2014**, *35*, 7898–7909. [CrossRef]

65. Duro, D.C.; Franklin, S.E.; Dubé, M.G. A comparison of pixel-based and object-based image analysis with selected machine learning algorithms for the classification of agricultural landscapes using SPOT-5 HRG imagery. *Remote Sens. Environ.* **2012**, *118*, 259–272. [CrossRef]

66. Pal, M.; Mather, P.M. An assessment of the effectiveness of decision tree methods for land cover classification. *Remote Sens. Environ.* **2003**, *86*, 554–565. [CrossRef]

67. Joshi, N.; Baumann, M.; Ehammer, A.; Fensholt, R.; Grogan, K.; Hostert, P.; Jepsen, M.; Kuemmerle, T.; Meyfroidt, P.; Mitchard, E.; et al. A Review of the application of optical and radar remote sensing data fusion to land use mapping and monitoring. *Remote Sens.* **2016**, *8*, 70. [CrossRef]

68. Abdikan, S.; Bilgin, G.; Sanli, F.B.; Uslu, E.; Ustuner, M. Enhancing land use classification with fusing dual-polarized TerraSAR-X and multispectral RapidEye data. *J. Appl. Remote Sens.* **2015**, *9*, 096054. [CrossRef]

69. Banks, S.; Millard, K.; Pasher, J.; Richardson, M.; Wang, H.; Duffe, J. Assessing the potential to operationalize shoreline sensitivity mapping: Classifying multiple wide fine quadrature polarized RADARSAT-2 and Landsat 5 scenes with a single Random Forest model. *Remote Sens.* **2015**, *7*, 13528–13563. [CrossRef]

70. Corcoran, J.; Knight, J.; Brisco, B.; Kaya, S.; Cull, A.; Murnaghan, K. The integration of optical, topographic, and radar data for wetland mapping in northern Minnesota. *Can. J. Remote Sens.* **2011**, *37*, 564–582. [CrossRef]

71. Balzter, H.; Cole, B.; Thiel, C.; Schmullius, C. Mapping CORINE land cover from sentinel-1A SAR and SRTM digital elevation model data using Random Forests. *Remote Sens.* **2015**, *7*, 14876–14898. [CrossRef]

72. Frazier, R.J.; Coops, N.C.; Wulder, M.A.; Kennedy, R. Characterization of aboveground biomass in an unmanaged boreal forest using Landsat temporal segmentation metrics. *ISPRS J. Photogramm. Remote Sens.* **2014**, *92*, 137–146. [CrossRef]

73. Midekisa, A.; Senay, G.B.; Wimberly, M.C. Multisensor earth observations to characterize wetlands and malaria epidemiology in Ethiopia. *Water Resour. Res.* **2014**, *50*, 8791–8806. [CrossRef] [PubMed]

74. Whiteside, T.; Bartolo, R. Mapping aquatic vegetation in a tropical wetland using high spatial resolution multispectral satellite imagery. *Remote Sens.* **2015**, *7*, 11664–11694. [CrossRef]

75. Breiman, L. Random Forests. *Mach. Learn.* **2001**, *45*, 5–32. [CrossRef]

76. Liaw, A.; Wiener, M. Classification and regression by randomForest. *R News* **2002**, *2*, 18–22.

77. Bivand, R.S.; Keitt, T.; Rowlingson, B. rgdal: Bindings for the Geospatial Data Abstraction Library, R Package Version 0.8-16. Available online: https://cran.r-project.org/web/packages/rgdal/index.html (accessed on 7 July 2017).

78. R Development Core Team. R: A Language and Environment for Statistical Computing. 2014. Available online: http://www.R-projec.org/ (accessed on 30 September 2016).

79. Liaw, A. Package "randomForest". Available online: http://cran.r-project.org/web/packages/randomForest/randomForest.pdf (accessed on 30 September 2016).

80. Millard, K.; Richardson, M.C. On the importance of training data sample selection in RF classification: A case study in peatland ecosystem mapping. *Remote Sens.* **2015**, *7*, 8489–8515. [CrossRef]

81. Congalton, R.G.; Green, K. *Assessing the Accuracy of Remotely Sensed Data: Principles and Practices*, 2nd ed.; Taylor & Francis: Didcot, UK, 2009; p. 192. ISBN 978-1-4200-5512-2.

82. Foody, G.M. Sample size determination for image classification accuracy assessment and comparison. *Int. J. Remote Sens.* **2009**, *30*, 5273–5291. [CrossRef]

83. Dingle Robertson, L.; King, D.J. Comparison of pixel- and object-based classification in land cover change mapping. *Int. J. Remote Sens.* **2011**, *32*, 1505–1529. [CrossRef]

84. Foody, G.M. Thematic map comparison: Evaluating the statistical significance of differences in classification accuracy. *Photogramm. Eng. Remote Sens.* **2004**, *70*, 627–633. [CrossRef]

85. Hapfelmeier, A.; Ulm, K. A new variable selection approach using Random Forests. *Comput. Stat. Data Anal.* **2013**, *60*, 50–69. [CrossRef]

86. Strobl, C.; Zeileis, A. Exploring the statistical properties of a test for Random Forest variable importance. In *COMPSTAT 2008—Proceedings in Computational Statistics*; Springer Science+Business Media: Berlin, Germany, 2008; pp. 59–66.

87. Pantaleoni, E.; Wynne, R.H.; Galbraith, J.M.; Campbell, J.B. Mapping wetlands using ASTER data: A comparison between classification trees and logistic regression. *Int. J. Remote Sens.* **2009**, *30*, 3423–3440. [CrossRef]

88. Skidmore, E.L.; Dickerson, J.D.; Schimmelpfennig, H. Evaluating surface-soil water content by measuring reflectance. *Soil Sci. Soc. Am. J.* **1975**, *39*, 238–242. [CrossRef]

89. Dronova, I. Object-Based image analysis in wetland research: A review. *Remote Sens.* **2015**, *7*, 6380–6413. [CrossRef]

90. Collins, S.L.; Knapp, A.K.; Briggs, J.M.; Blair, J.M.; Steinauer, E.M. Modulation of diversity by grazing and mowing in native tallgrass prairie. *Science* **1998**, *280*, 745–747. [CrossRef] [PubMed]

91. Heisler, J.L.; Briggs, J.M.; Knapp, A.K. Long-term patterns of shrub expansion in a C4-dominated grassland: Fire frequency and the dynamics of shrub cover and abundance. *Am. J. Bot.* **2003**, *90*, 423–428. [CrossRef] [PubMed]

92. Jones, J.W.; Hall, A.E.; Foster, A.M.; Smith, T.J.I. Wetland fire scar monitoring and analysis using archival landsat data for the everglades. *Fire Ecol.* **2013**, *9*, 133–150. [CrossRef]

93. Li, G.; Lu, D.; Moran, E.; Dutra, L.; Batistella, M. A comparative analysis of ALOS PALSAR L-band and RADARSAT-2 C-band data for land-cover classification in a tropical moist region. *ISPRS J. Photogramm. Remote Sens.* **2012**, *70*, 26–38. [CrossRef]

94. Mayaux, P.; Grandi, G.F.D.; Rauste, Y.; Simard, M.; Saatchi, S. Large-scale vegetation maps derived from the combined L-band GRFM and C-band CAMP wide area radar mosaics of Central Africa. *Int. J. Remote Sens.* **2002**, *23*, 1261–1282. [CrossRef]

95. Corcoran, J.M.; Knight, J.F.; Gallant, A.L. Influence of multi-source and multi-temporal remotely sensed and ancillary data on the accuracy of Random Forest classification of wetlands in northern Minnesota. *Remote Sens.* **2013**, *5*, 3212–3238. [CrossRef]

96. Na, X.; Zang, S.; Wang, J. Evaluation of Random Forest ensemble classification for land cover mapping using TM and ancillary geographical data. In Proceedings of the Sixth International Conference on Fuzzy Systems and Knowledge Discovery, Tianjin, China, 14–16 August 2009; pp. 89–93.

97. Davranche, A.; Lefebvre, G.; Poulin, B. Wetland monitoring using classification trees and SPOT-5 seasonal time series. *Remote Sens. Environ.* **2010**, *114*, 552–562. [CrossRef]

98. Baker, C.; Lawrence, R.L.; Montagne, C.; Patten, D. Change detection of wetland ecosystems using Landsat imagery and change vector analysis. *Wetlands* **2007**, *27*, 610–619. [CrossRef]

99. Wright, C.; Gallant, A. Improved wetland remote sensing in Yellowstone National Park using classification trees to combine TM imagery and ancillary environmental data. *Remote Sens. Environ.* **2007**, *107*, 582–605. [CrossRef]

100. Souza-Filho, P.W.M.; Paradella, W.R.; Rodrigues, S.W.P.; Costa, F.R.; Mura, J.C.; Gonçalves, F.D. Discrimination of coastal wetland environments in the Amazon region based on multi-polarized L-band airborne Synthetic Aperture Radar imagery. *Estuar. Coast. Shelf Sci.* **2011**, *95*, 88–98. [CrossRef]

101. Bourgeau-Chavez, L.L.; Kowalski, K.P.; Carlson Mazur, M.L.; Scarborough, K.A.; Powell, R.B.; Brooks, C.N.; Huberty, B.; Jenkins, L.K.; Banda, E.C.; Galbraith, D.M.; et al. Mapping invasive Phragmites australis in the coastal Great Lakes with ALOS PALSAR satellite imagery for decision support. *J. Great Lakes Res.* **2013**, *39*, 65–77. [CrossRef]

102. Koch, M.; Schmid, T.; Reyes, M.; Gumuzzio, J. Evaluating full polarimetric C- and L-band data for mapping wetland conditions in a semi-arid environment in Central Spain. *IEEE J. Sel. Top. Appl. Earth Obs. Remote Sens.* **2012**, *5*, 1033–1044. [CrossRef]

103. Touzi, R.; Deschamps, A.; Rother, G. Wetland characterization using Polarimetry RADARSAT-2 capability. *Can. J. Remote Sens.* **2007**, *33*, S56–S67. [CrossRef]

104. Brisco, B.; Schmitt, A.; Murnaghan, K.; Kaya, S.; Roth, A. SAR polarimetric change detection for flooded vegetation. *Int. J. Digit. Earth* **2013**, *6*, 103–114. [CrossRef]

105. Strobl, C.; Malley, J.; Tutz, G. An introduction to recursive partitioning: Rationale, application, and characteristics of classification and regression trees, bagging, and Random Forests. *Psychol. Methods* **2009**, *14*, 323–348. [CrossRef] [PubMed]

106. Bernard, S.; Adam, S.; Heutte, L. Dynamic Random Forests. *Pattern Recog. Lett.* **2012**, *33*, 1580–1586. [CrossRef]

107. Janitza, S.; Strobl, C.; Boulesteix, A.-L. An AUC-based permutation variable importance measure for random forests. *BMC Bioinform.* **2013**, *14*, 119. [CrossRef] [PubMed]

108. Castilla, G. We must all pay more attention to rigor in accuracy assessment: Additional comment to "The improvement of land cover classification by thermal remote sensing". *Remote Sens.* **2016**, *8*, 8368–8390. [CrossRef]